Optics Letters

Characterization of pixelated nanogratings in 3D holographic display by an imaging Mueller matrix ellipsometry

Chao Chen,[1] Xiuguo Chen,[1,3] Zhongwen Xia,[2] Jiacheng Shi,[2] Sheng Sheng,[1] Wen Qiao,[2,4] and Shiyuan Liu[1]

[1]State Key Laboratory of Digital Manufacturing Equipment and Technology, Huazhong University of Science and Technology, Wuhan 430074, China
[2]School of Optoelectronic Science and Engineering & Collaborative Innovation Center of Suzhou Nano Science and Technology, Soochow University, Suzhou 215006, China
[3]e-mail: xiuguochen@hust.edu.cn
[4]e-mail: wqiao@suda.edu.cn

Received 30 March 2022; revised 24 May 2022; accepted 27 June 2022; posted 27 June 2022; published 13 July 2022

The diffraction grating, as an element that can control the direction of the emitted light, is the key component used in holographic sampling three-dimensional (3D) displays. The structural accuracy of nanogratings greatly affects the precision of light modulation, thus influencing the cross talk and resolution in 3D displays. It is of great significance for the nondestructive measurement of nanogratings. However, existing measurement methods have certain limitations such as destructiveness and low measurement efficiency in the face of measuring such pixelated nanogratings. In this work, aimed at the measurement requirements and challenges of pixelated nanogratings in 3D displays, we propose to use a self-designed imaging Mueller matrix ellipsometer (IMME) for grating characterization. A sample containing 6 periods and 10 orientations of pixelated gratings is investigated to verify the effectiveness of the method used. Through the measurement and fitting data, the measurement data obtained by using the IMME can be well matched with the theoretical results. At the same time, the extraction results of the structural parameters, periods, and orientations are also consistent with the measurement results from scanning electron microscopy. It is expected that the IMME will provide a guarantee for the accurate display of 3D holography.

https://doi.org/10.1364/OL.459522

Introduction. Vision is the most important way for humans to perceive the objective world and obtain external information. As an important technology for the intuitive presentation of visual information, display technology is committed to the most realistic restoration of the information in the objective world, which is of great significance to meet the visual needs of human beings. As an effective means, the three-dimensional (3D) display technology has received extensive attention because it provides users with vivid 3D images without any visual aids [1–3]. Among them, the 3D display technology based on diffractive optics mainly adopts holographic optical elements, nanograting structures, etc., which can control the direction of the emitted light precisely over an ultrawide tuning range, and can achieve better display effects [4].

Many studies have been performed on the use of diffractive optics to achieve 3D displays. In 2010, Chen *et al*. proposed for the first time the use of diffractive optical elements to realize autostereoscopic display [5]. In 2014, Hwang *et al*. proposed that volume holographic optical elements should be used in time-division multiplexed autostereoscopic display [6]. In 2013, Fattal *et al*. proposed the use of a directional backlight structure to control the direction of the emitted light, which is composed of pixelated nanogratings [7]. Most recently, foveated glasses-free 3D displays using a two-dimensional metagrating complex was proposed to provide a record viewing angle of 160° [8,9]. In nanograting based 3D displays, the view distribution is determined by the period and orientation of the grating pixels. In this 3D display technology, the high-precision preparation of nanogratings is the basis for realizing light directivity modulation, and the measurement of the period, orientation, and structural parameters of the pixelated nanogratings is therefore particularly important.

However, it is quite challenging to measure the nanograting matrix in 3D displays. First, there are more than 10^7 nanogratings in a typical 3D display system. Since the orientation and period of each grating is different from each other, a non-destructive measuring method with reasonable throughput is required. Second, the pixel size of each nanograting is in the range of 10–50 μm, making the measurement an even harder task. Third, the periodic variation of each nanograting is on the nanometer scale. A precise measurement approach should be explored to detect the subtle structural difference.

There are a few traditional measurement methods that can be used for the measurement of the grating structure parameters, such as atomic force microscopy, scanning electron microscopy (SEM), and transmission electron microscopy. However, these technologies cannot satisfy the non-destructive measurement of grating structure parameters.

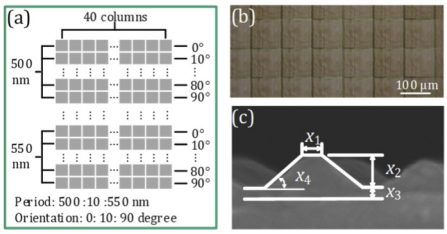

Fig. 1. (a) Schematic diagram of pixel arrangement, (b) optical micrograph, and (c) SEM image and modeling parameter setting of the pixelated grating sample.

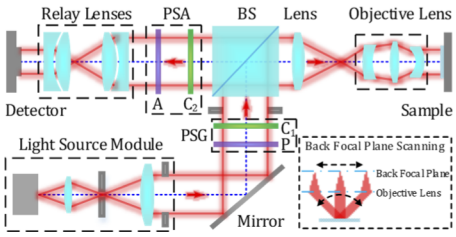

Fig. 2. Schematic diagram for the tomographic imaging Mueller matrix ellipsometry. Inset shows the principle of back focal plane scanning. P, polarizer; C_1, the 1st rotating compensator; BS, beam splitter; C_2, the 2nd rotating compensator; A, analyzer; PSG, polarization state generator; PSA, the polarization state analyzer.

Ellipsometry is a technique that uses the change of polarization state of light to analyze samples. It has the advantages of non-destructiveness, ultrahigh sensitivity, and no need for reference materials [10]. Ellipsometry has currently developed as an important tool for thin-film characterization, and has also been successfully extended for the measurement of nanostructures, such as etched Si gratings [11], holographic gratings [12], and gate-all-around transistor structures [13]. However, since the traditional ellipsometry requires the sample size to be larger than the system spot, there are certain limitations when it comes to the measurement problem of pixelated nanogratings in 3D displays.

In this work, aimed at the measurement requirements and challenges of pixelated nanogratings in 3D displays, we propose to use a self-designed imaging Mueller matrix ellipsometer (IMME) for characterization. The IMME has the ability to achieve high precision ellipsometric measurement while achieving high lateral resolution of pixelated nanogratings. In addition, with the IMME, the structural parameters, orientation, and period of the pixelated grating can also be measured at the same time.

Sample description. The sample studied is a pixelated grating with different periods and orientations in 3D displays, manufactured by self-developed spatial frequency variable photolithography (Nanocrystal 200, SVG Corporation) [14,15] made by Soochow University, as shown in Fig. 1.

Figure 1(a) is a schematic diagram of the pixel arrangement of the grating. The size of the entire sample area is approximately 4 mm × 6 mm, and there are 60 rows of pixels in the entire format. Each row has 40 pixelated grating areas. All pixels are closely arranged. The size of a single pixelated grating area is 100 μm × 100 μm. The period and orientation of the 40 pixelated gratings in each row are the same. For different lines, from top to bottom, the period is the same every ten lines, there are 6 kinds of periods, from 500 nm to 550 nm, changing at 10 nm intervals. In ten rows of pixels with the same period, from top to bottom, the orientation changes from 0° to 90°, changing at 10° intervals. Figure 1(b) is an optical micrograph of the pixelated grating sample. To fit the grating, four parameters will be used to describe the grating: critical dimension x_1, line height x_2, thickness of residual layer x_3, and sidewall angle x_4, as shown in Fig. 1(c).

The material used for the measured grating is a photoresist. It is achieved by spin-coating a tackifier on a quartz substrate, and then coating the photoresist on it. Laser interference lithography technology was used to realize the preparation of nanostructures. Before measuring the nanostructures, it is still necessary to determine the optical constants of the materials used in the nanostructures. Through the measurement and analysis of the quartz substrate and the quartz substrate with the spin-coated tackifier, we found that the thickness of the tackifier is too thin and will not have any effect on the spectrum of the quartz plate. Details can be found in Supplement 1. Therefore, in the subsequent analysis, the influence of the tackifier on the spectrum will be ignored. The fitting results of optical constants of the photoresist can be found in Supplement 1.

Method. Figure 2 shows the basic optical principle of the IMME. The main components of the IMME include two parts: the ellipsometric measurement part and microscopy imaging part. The ellipsometric measurement optical path adopts the classic design of the traditional dual-rotating compensator Mueller matrix ellipsometer, and the microscopy imaging optical path is designed based on the optical path of the orthoscopic illumination mode microscope [16,17].

A monochromatic filter is used in the light source module to filter the light of the white-light source into monochromatic light, and the detection of the information of the sample in the spectral dimension is realized by wavelength scanning. The polarization state generator (PSG) and the polarization state analyzer (PSA) are both composed of a polarizer (linear polarizer) and a rotating self-designed compensator [18]. The former is used to convert non-polarized incident light into linearly polarized light with a fixed polarization direction, and the latter is used to modulate linearly polarized light into differently polarized light whose polarization state changes with time. In the IMME, the rotation compensator ratio of compensators in the PSG and PSA is 5:3.

To ensure the highest sensitivity, different samples need to be measured at the incidence angle and orientation, where the polarization is most sensitive. To realize different incident angles, a back focal plane scanning optical path is designed, as shown in the insert in Fig. 2. By changing the angle of the mirror, the position of the convergent point of the light beam on the back focal plane of the objective lens will be changed, and then the incident angle of the system will be changed. Furthermore, by employing a high numerical aperture objective lens, the IMME can achieve lateral resolution better than 0.8 μm in the working wavelength range [17]. The detailed data acquisition process can be found in Supplement 1.

The light passing through the IMME is collected by the detector, and the expression of the intensity vector collected for multiple times can be written as the following formulas:

$$\mathbf{I} = \mathbf{AMG}, \tag{1}$$

$$\mathrm{vec}(\mathbf{I}) = \mathbf{D}\mathrm{vec}(\mathbf{M}). \tag{2}$$

Here, **G** is the sets of columnar Stokes vectors representing the PSG, **A** is the set of row Stokes vectors representing the

PSA, and **M** represents the 4th-order Mueller matrix of the sample between the PSG and the PSA. The vec(·) represents the vectorization operator of the matrix. The matrix **D** contains the information of **G** and **A**, and can be obtained through the instrument system calibration [17].

Extracting the parameters of the nanostructure to be measured from the Mueller matrix of the sample is a typical inverse problem-solving process. It mainly depends on two key technologies: one is the forward optical characteristic modeling and its fast solution method; the other is the reverse geometric feature parameter solution and its fast algorithm. The theoretical Mueller matrix of periodic nanostructures can be solved using the rigorous coupled-wave analysis (RCWA) method and electromagnetic propagation theory [19,20]. First, the IMME is used to measure the sample and obtain the light intensity signal at certain incidence angles and orientations, then the corresponding measurement Mueller matrix **M** is obtained. Second, the RCWA model and electromagnetic propagation theory are used to calculate and obtain the theoretical Mueller matrix **Mc** of the sample, according to the initial value of the parameter to be measured, the optical constant of the sample material, and the measured incident angle. Finally, through the least squares regression analysis algorithm, the parameters to be measured are continuously changed in the iterative process until the calculated results and the measured data match as much as possible. Then, the structural parameters input into the system are the extracted nanostructure measurement results. This process is shown in Fig. 3. In the process of parameter extraction, an evaluation function in the form of χ^2 is often used to evaluate the fitting error between the measured and calculated Mueller matrix elements:

$$\chi^2 = \frac{1}{15N - P}\sum_{k=1}^{N}\sum_{i,j=1}^{4}\left[\frac{m_{ij,k}^{\mathrm{mea}} - m_{ij,k}^{\mathrm{calc}}}{\sigma(m_{ij,k}^{\mathrm{mea}})}\right]^2. \tag{3}$$

Here, $m_{ij,k}^{\mathrm{mea}}$ and $m_{ij,k}^{\mathrm{calc}}$ are the elements in **M** and **Mc**, respectively. The subscripts i and j represent the Mueller matrix element index, and the element m_{11} is not included here ($_{ij,k}m_{11} \equiv 1$); k represents the spectral point index and N is the total number of spectral points; $\sigma(m_{ij,k}^{\mathrm{mea}})$ is the standard deviation of the measured Mueller matrix elements. Additionally, P is the number of parameters to be measured. The detailed modeling method can be found in Supplement 1.

Results. Figure 4 shows one of a series of images acquired by the IMME at a wavelength of 630 nm. Each point of the measured image corresponds to a micro-area on the sample. Selecting regions or points from the acquired images enables independent

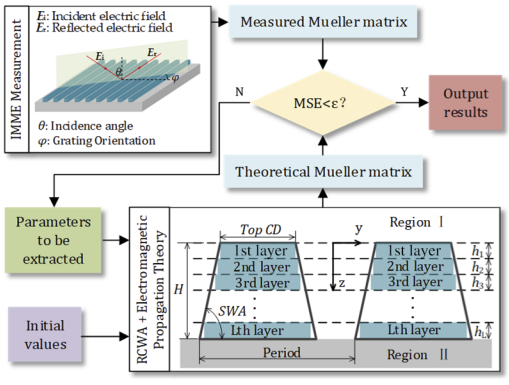

Fig. 3. Flow chart of system parameter iterative solution.

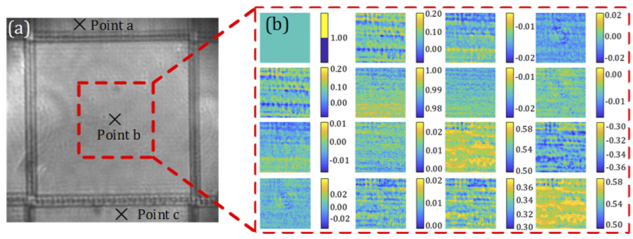

Fig. 4. (a) Sample image collected by IMME at 630 nm; (b) imaging Mueller matrix corresponding to the red dotted box shown in panel (a).

Table 1. Parameter Extraction Results from the IMME of Pixelated Gratings in Fig. 4 (95% Confidence Limits)

Point Letter	a	b	c
Nominal period/nm	530	530	540
Nominal orientation/°	80	90	0
Period/nm	532.6 ± 4.52	533.1 ± 3.54	538.5 ± 5.19
Orientation/°	80.2 ± 0.48	89.5 ± 0.32	0.3 ± 0.25
x_1/nm	84.7 ± 1.12	83.8 ± 2.25	83.2 ± 2.51
x_2/nm	178.8 ± 3.65	181.2 ± 4.21	187.6 ± 3.25
x_3/nm	146.5 ± 4.32	148.7 ± 3.20	135.8 ± 5.21
x_4/°	51.2 ± 1.53	50.8 ± 0.89	52.1 ± 1.25

analysis. Figure 4(b) is the Mueller matrix of the sample calculated by the red dotted box shown in Fig. 4(a). By fitting and analyzing the measured Mueller matrix, the topographic parameters of the corresponding area of the sample can be obtained. The grating parameters extracted from the three crossed points in Fig. 4(a) are given in Table 1. It should be pointed out that the uncertainty of orientation has nothing to do with the absolute magnitude of the true value, but only represents the deviation from the true data.

Figure 5 shows the measurement fitting results of the pixelated nanogratings at point a shown in Fig. 4(a) at wavelengths of 450–700 nm. It can be seen from the figure that the measurement and fitting results can be accurately matched. Moreover, since the orientation of the grating is no longer zero, the values of the 2×2 off diagonal Mueller matrix elements are no longer zero. It can also be seen from the figure that light with a wavelength greater than 600 nm is more sensitive to changes in the structural parameters and can be used to quickly identify changes in the pixelated grating parameters. Also in this range, the anisotropy of the grating structure due to the orientation can also be clearly reflected from the results. Although using multi-azimuth-angle data during the fitting process will make the extracted results

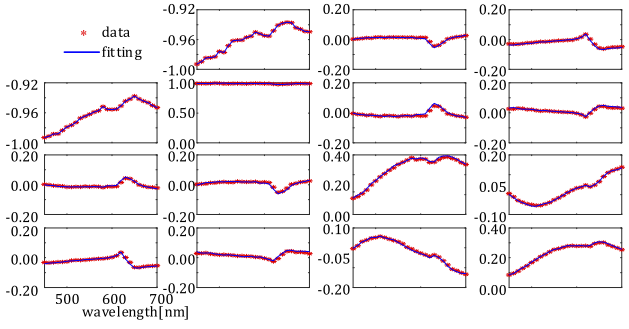

Fig. 5. Measurement and fitting results of the pixelated nanogratings at point a shown in Fig. 4(a).

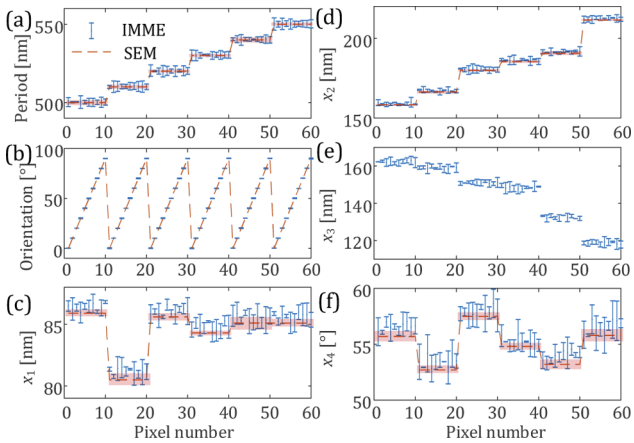

Fig. 6. (a) Period, (b) orientation, (c) x_1, (d) x_2, (e) x_3, and (f) x_4 extraction results (95% confidence limits) from IMME and SEM. The red area represents the uncertainty of SEM measurements.

more accurate [21], we use the single-azimuth-angle data for parameter extraction to improve the efficiency of the measurement and analysis under the premise of ensuring accuracy via experimental verification. Details can be found in Supplement 1.

We investigated samples with different regions with the same period and orientation, and then calculated the uncertainty of the measured parameters of each structure, as shown in Fig. 6. The SEM-measured values including uncertainties were estimated by manually measuring the SEM micrographs. Pixelated gratings with different orientations and the same periods share the same SEM measurement results because they are fabricated with the same settings. Here, the comparison results of orientation and period (dashed line) are nominal values. As can be seen from the figure, the SEM measurements of most parameters are in good agreement with the IMME results. There are some points of inconsistency, because the actual values of the parameters at the time of manufacture have a certain difference.

Conclusion. Using the self-developed tomographic Mueller matrix ellipsometer, pixelated gratings in 3D displays were measured. To ensure the accuracy of the measurement and analysis of the grating structure, the period and structural parameters of the grating can be obtained at the same time during the measurement with the IMME. With the characteristics of high lateral resolution, the required area can be selected to reconstruct its respective morphological parameters by solving the inverse problem. The data of the entire detection surface can be obtained and analyzed separately at the same time. Compared to a traditional ellipsometer, the measurement efficiency of large-area samples is greatly improved. The extracted parameters are compared and analyzed with SEM methods, and the consistency of the results shows the potential ofimaging Mueller matrix ellipsometry in the application of 3D holographic display measurement.

Funding. National Natural Science Foundation of China (51727809, 62175075, 52022034, 52130504); Key Research and Development Plan of Hubei Province (2020BAA008).

Disclosures. The authors declare no conflicts of interest.

Data availability. Data underlying the results presented in this paper are not publicly available at this time but may be obtained from the authors upon reasonable request.

Supplemental document. See Supplement 1 for supporting content.

REFERENCES

1. H. Jang, J. Lee, G. Baek, J. Kwak, and J. Park, J. Inform. Display **23**, 1 (2022).
2. J. Park and B. Lee, Light: Adv. Manuf. **3**, 1 (2022).
3. Y. Deng and D. Chu, Sci. Rep. **7**, 1 (2017).
4. J. Hua, D. Yi, W. Qiao, and L. Chen, Opt. Commun. **472**, 125829 (2020).
5. C. Y. Chen, Q. L. Deng, and H. C. Wu, Displays **31**, 169 (2010).
6. Y. S. Hwang, F. K. Bruder, T. Fäcke, S. C. Kim, G. Walze, R. Hagen, and E. S. Kim, Opt. Express **22**, 9820 (2014).
7. D. Fattal, Z. Peng, T. Tran, S. Vo, M. Fiorentino, J. Brug, and R. G. Beausoleil, Nature **495**, 348 (2013).
8. J. Hua, E. Hua, F. Zhou, J. Shi, C. Wang, H. Duan, Y. Hu, W. Qiao, and L. Chen, Light: Sci. Appl. **10**, 1 (2021).
9. J. Shi, W. Qiao, J. Hua, R. Li, and L. Chen, Nanophotonics **9**, 3003 (2020).
10. H. Fujiwara, "*Spectroscopic Ellipsometry Principles and Applications*," (John Wiley & Sons Inc., 2007), Chap. 4, pp. 87–117.
11. H. T. Huang and F. L. Terry, Thin Solid Films **455-456**, 828 (2004).
12. T. Novikova, A. De Martino, P. Bulkin, Q. Nguyen, B. Drévillon, V. Popov, and A. Chumakov, Opt. Express **15**, 2033 (2007).
13. A. C. Diebold, A. Antonelli, and N. Keller, APL Mater. **6**, 058201 (2018).
14. W. Wan, W. Qiao, W. Huang, M. Zhu, Z. Fang, and D. Pu, Opt. Express **24**, 6203 (2016).
15. Y. Ye, F. Xu, G. Wei, Y. Xu, D. Pu, and L. Chen, Opt. Lett. **42**, 1978 (2017).
16. C. Chen, X. Chen, H. Gu, H. Jiang, C. Zhang, and S. Liu, Meas. Sci. Technol. **30**, 025201 (2019).
17. C. Chen, X. Chen, C. Wang, S. Sheng, L. Song, H. Gu, and S. Liu, Opt. Express **29**, 32712 (2021).
18. H. Gu, X. Chen, H. Jiang, Y. Shi, and S. Liu, Opt. Lett. **44**, 3026 (2019).
19. M. G. Moharam, E. B. Grann, and D. A. Pommet, J. Opt. Soc. Am. A **12**, 1068 (1995).
20. L. Li, J. Opt. Soc. Am. A **13**, 1870 (1996).
21. M. Foldyna, A. De Martino, E. Garcia-Caurel, R. Ossikovski, C. Licitra, F. Bertin, K. Postava, and B. Drevillon, Eur. Phys. J. Appl. Phys. **42**, 351 (2008).